Enhanced surface warming and accelerated snow melt in the Himalayas and Tibetan Plateau induced by absorbing aerosols

Environ. Res. Lett. **5** (2010) 025204 (10pp) doi:10.1088/1748-9326/5/2/025204

Enhanced surface warming and accelerated snow melt in the Himalayas and Tibetan Plateau induced by absorbing aerosols

William K M Lau[1], Maeng-Ki Kim[2], Kyu-Myong Kim[3] and Woo-Seop Lee[2]

[1] Laboratory for Atmospheres, NASA Goddard Space Flight Center, Greenbelt, MD 20771, USA
[2] Department of Atmospheric Science, Kongju National University, Gongju, 314-701, Korea
[3] Goddard Earth Sciences and Technology Center, University of Maryland Baltimore County, Baltimore, MD 21228, USA

E-mail: William.k.lau@nasa.gov, mkkim@konju.ac.kr, Kyu-Myong.Kim@nasa.gov and wooseobi@kongju.ac.kr

Received 25 November 2009
Accepted for publication 20 January 2010
Published 9 April 2010
Online at stacks.iop.org/ERL/5/025204

Abstract
Numerical experiments with the NASA finite-volume general circulation model show that heating of the atmosphere by dust and black carbon can lead to widespread enhanced warming over the Tibetan Plateau (TP) and accelerated snow melt in the western TP and Himalayas. During the boreal spring, a thick aerosol layer, composed mainly of dust transported from adjacent deserts and black carbon from local emissions, builds up over the Indo-Gangetic Plain, against the foothills of the Himalaya and the TP. The aerosol layer, which extends from the surface to high elevation (∼5 km), heats the mid-troposphere by absorbing solar radiation. The heating produces an atmospheric dynamical feedback—the so-called elevated-heat-pump (EHP) effect, which increases moisture, cloudiness, and deep convection over northern India, as well as enhancing the rate of snow melt in the Himalayas and TP. The accelerated melting of snow is mostly confined to the western TP, first slowly in early April and then rapidly from early to mid-May. The snow cover remains reduced from mid-May through early June. The accelerated snow melt is accompanied by similar phases of enhanced warming of the atmosphere–land system of the TP, with the atmospheric warming leading the surface warming by several days. Surface energy balance analysis shows that the short-wave and long-wave surface radiative fluxes strongly offset each other, and are largely regulated by the changes in cloudiness and moisture over the TP. The slow melting phase in April is initiated by an effective transfer of sensible heat from a warmer atmosphere to land. The rapid melting phase in May is due to an evaporation–snow–land feedback coupled to an increase in atmospheric moisture over the TP induced by the EHP effect.

Keywords: water cycle, enhanced warming and accelerated melting of glacier in Himalayas and the Tibetan Plateau

S Online supplementary data available from stacks.iop.org/ERL/5/025204/mmedia

1. Introduction

The Tibetan Plateau (TP)—the 'Roof of the World'—exerts profound influences not only on the Asian monsoon large scale circulation through its dynamical and thermal forcing (Manabe and Broccoli 1990, Yanai *et al* 1992, Yanai and Wu 2006), but also on the water cycle of the entire Asian continent. The seasonal melting of snowpack and mountain glaciers feeds the seven major rivers of Asia, the Yangtze, the Yellow River, the Ganges, the Indus, the Brahmaputra, the Salween, and the Mekong, providing the fresh water supply to a large portion of the population of Asia. In this regard, the TP could be aptly called the 'Water Tower of Asia'. In recent years, there has been growing evidence of increased warming, accompanied by early snow melt, and retreat of high mountain glaciers in the Himalayas and the TP regions (IPCC 2007, He *et al* 2003, Jain 2008, Ren *et al* 2006, Kulkarni *et al* 2007, Liu and Chen 2000, Shrestha *et al* 1999 and many others). Particularly in the western and central Himalayas, the rate of retreat has been increasing in recent decades (Raina and Sangewar 2007, Jain 2008). The early snow melt and rapid retreat of glaciers in the Himalayas and TP pose serious and unprecedented threats to the fresh water supply of the entire Asia population (Kehrwald *et al* 2008). Already glacier melt has led to soil erosion, bursting of glacier lakes, with devastating floods in Himalaya countries such as Nepal and Bhutan (Shrestha *et al* 1999).

Up to now, the warming and the accelerated glacier melt in the Himalayas and TP have been attributed to greenhouse warming (Duan *et al* 2006, Oerlemans 2005, Kulkarni *et al* 2002, Ren *et al* 2006). Yet, the greenhouse warming rate is of the order of 0.1–0.15 K/decade, whereas the warming of the TP has been estimated to be much faster, at 0.32 K/decade (Liu and Chen 2000). Over the Himalaya foothill regions and Middle Mountain regions in Nepal, the warming rate is even faster, estimated at 0.7–1.2 °C per decade since 1977–94 (Shrestha *et al* 1999). Based on these differences in warming rates, it may be argued that greenhouse warming is not necessarily the sole agent of change in these regions, and that local forcing and feedback processes could play an important role in causing the faster warming rate, and accelerated retreat of the mountain glaciers.

Many factors besides greenhouse warming could have led to accelerated warming over the Himalayas and TP. These include increased land-use and land change, increased sunlight duration from reduction in cloudiness, increased water vapor feedback, and reduction of snow albedo by deposition of soot and dust on the snow surface (Kang *et al* 2000, Prasad and Singh 2007, Flanner *et al* 2007, 2009, Yasunari *et al* 2009). Recently Ramanathan *et al* (2007) estimated that atmospheric heating by Asian brown clouds (ABCs) doubles the greenhouse warming over South Asia, and may contribute substantially to the loss of glacier mass in the Himalayas. In contemporary papers, Lau *et al* (2006), Lau and Kim (2006) and Lau *et al* (2008) proposed the 'elevated heat pump' (EHP) mechanism, by which absorbing aerosols may affect the South Asian monsoon. They demonstrated that dust and black carbon transported to high altitude in the Himalayas and TP region in boreal spring can induce upper tropospheric heating over the TP through atmospheric feedback processes, leading to enhanced rainfall in the Himalayan foothills in the late spring and early summer. Long-term upper tropospheric warming consistent with the EHP hypothesis has been observed over the western Himalayas (Gautam *et al* 2009, Prasad *et al* 2009). In this paper, we will investigate the impact of atmospheric heating by dust and black carbon in possibly leading to enhanced pre-summer monsoon surface warming and early snow melt in the Himalayas and TP region. The snow-darkening effect by black carbon and dust is not considered in the present study.

2. Experimental design

The results of this paper are based on numerical experiments using the NASA fvGCM (Lin 2004, Atlas *et al* 2005) with the Microphysics with Relaxed Arakawa–Schubert (McRAS) parametrization of atmospheric moist processes, which include state-of-the-art prognostic cloud water schemes, and liquid-and ice-phase cloud microphysics (Sud and Walker 1999, 2003), and the radiative transfer scheme of Chou and Suarez (1994, 1999). The fvGCM has a $2 \times 2.5°$ resolution, 55 layers in the vertical, and is coupled to the NCAR community land model (Dai *et al* 2002) and a perturbation mixed layer ocean (MLO) model (Waliser *et al* 1999). Global aerosol loading is prescribed from monthly climatologies (interpolated to daily values) of four-dimensional distributions of each of the five aerosol species (dust, black carbon, organic carbon, sulfate, and sea salt) derived from the Goddard Chemistry Aerosol Radiation Transport (GOCART) model (Chin *et al* 2002, 2004). The extinction coefficient, single-scattering albedo, and asymmetry factor for each aerosol type are computed for 11 broad wavelength bands from Mie theory as a function of the ambient relative humidity. Both short-wave and long-wave forcing are included. The GOCART dust model uses eight particle sizes ranging from 0.1 to 10 μm, and a dust generating parametrization, which is a function of the surface wind, soil types and surface depression (Ginoux *et al* 2001). Dust single-scattering albedo (SSA) used in the model has a range from 0.8 to 0.94 in the short-wave spectral range (0.4–2.27 μm). These SSA values represent moderate-to-strong absorbing dust aerosols, and are consistent with recent observations of dust absorptivity over the Indo-Gangetic Plain (Ramana *et al* 2004). For black carbon and organic carbon, the SSA at visible wavelengths is a function of relative humidity, ranging from 0.21 for the very dry case to 0.53 for the saturated case for black carbon and 0.96–0.99 for organic carbon. Sea salt and sulfate are highly reflecting aerosols, with an SSA at visible wavelengths of unity. The aerosol properties are also influenced by the simulated model humidity, so that there is some degree of feedback between the aerosol properties and the model climate variables. However, this effect is relatively small compared to the spectral range of the optical properties.

To identify the mechanism of aerosol impacts, two sets of four-member ensemble experiments with different initial conditions have been carried out, first with all aerosols included (AA) and second with no aerosol forcing (NA), for eight years (2000–2007) from 1 April to 31 October. The

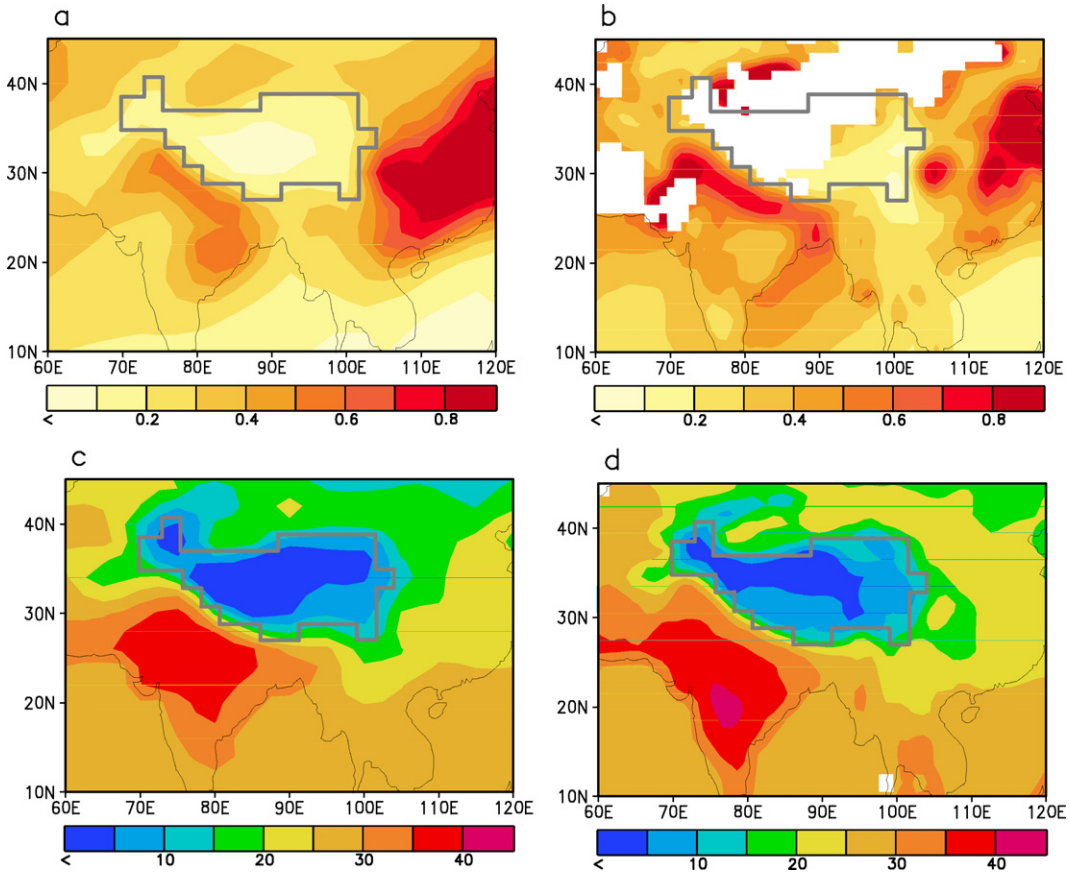

Figure 1. Spatial distribution of May monthly mean model climatology of (a) aerosol optical thickness (AOD) and (c) air temperature (°C) from control run (NA), compared with corresponding observed climatology of (b) MODIS AOD (from 2000 to 2009) and (d) air temperature from AIRS (from 2003 to 2009). The model outline of the TP is shown by the solid gray line.

carbon dioxide concentration is identical in all experiments. An anomaly is defined as the difference between the AA and NA (AA-minus-NA) ensembles. Because the initial and boundary forcing are identical in the two sets of experiments, and because the ensemble climatology consists of a large number ($32 = 4 \times 8$) of members, the internal variability is much reduced, so that the anomalies can be attributed largely to response of the water cycle to aerosol forcing. For all anomalies, we have computed point-wise, pooled t-tests for statistical significance based on the ensembles of AA and NA experiments.

3. Results

3.1. Warming over the TP and the EHP effect

During the pre-monsoon season, April–May, aerosols from dust transport, biomass and biofuel burning, and industrial activities rapidly build up over the Indo-Gangetic Plain (IGP) and East Asia (figure 1(a) for May). The highest AOD (>0.8) from GOCART is found over central and northeastern China. Over South Asia, aerosol loading is high (AOD >0.4) in the IGP, and around the slopes of the TP, as evident in the 0.2 AOD contour outlining the topographic contour of the TP. Compared to the observed AOD (figure 1(b)) from the moderate resolution imaging spectro-radiometer (MODIS), the GOCART AOD has a reasonable distribution in the IGP, except that the model seems to have under-estimated the AOD by about 20–30% over the IGP (see table 1), especially in northwestern India (Yu *et al* 2010). Over East Asia, the total AOD is comparable in magnitude, but lacks the finer features in MODIS. Because of the bright surface of the TP, the satellite retrieval of AOD over the TP is highly uncertain and is not included as part of the standard MODIS data. The near-surface (2 m) air temperature climatology simulated by the model (AA) shows a temperature difference of over 50°C between the top of the TP and the land region of northern India, with a large gradient along the foothills of the Himalayas. These features are quite similar to the surface air temperature from the atmospheric infra-red sounder (AIRS), except for the extreme hotspot (>40°C) over central India, which is not well simulated by the model. The broad similarity of the model AOD and surface temperature to observations provide assurance of the realism of the model simulations.

Examination of the composition of the aerosols from GOCART (table 1) indicates that, over the Indian continent, a substantial portion (∼57%) of the AOD is from the absorbing types, i.e. dust and black carbon, while the high concentration over East Asia is primarily due to sulfates (62%). As a response to the aerosol forcing, a large surface cooling anomaly of 1–2 °C is found over all land regions of India (figure 2), due

Table 1. Mean aerosol optical depth (AOD) and the percentage contributions from each of five aerosol species used in this study averaged over the Indo-Gangetic Plain (IGP), TP, and Central China, for the month of May. MODIS AOD is undefined over the TP.

	IGP (25–30° N, 75–85° E)	TP (30–35° N, 80–95° E)	Central China (25–35° N, 105–120° E)
GOCART	0.41	0.14	0.73
MODIS	0.65	—	0.61
Black carbon (%)	1.6	10.4	8.0
Dust (%)	45.2	44.4	16.8
Sulfate (%)	16.7	22.2	62.0
Organic carbon (%)	24.1	19.4	12.3
Sea salt (%)	2.5	2.1	1.0

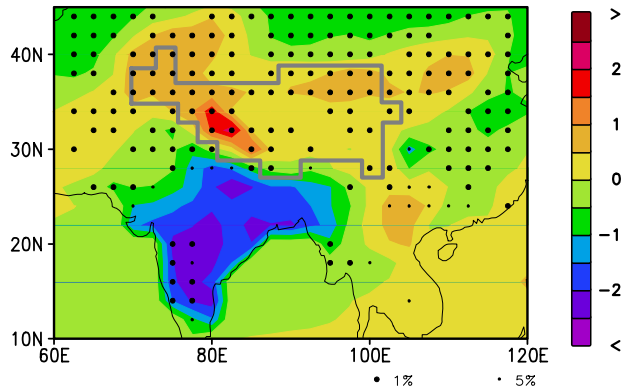

Figure 2. Spatial distribution of simulated difference of surface skin temperature (°C) between AA and NA runs for the month of May. Grid points with statistical confidence levels exceeding 5 and 1% are indicated by small and large closed circles, respectively. The model outline of the Tibetan Plateau is shown by a solid gray line.

to the combined effect of high AOD and increased cloud shielding (see following discussion). Similarly, over East Asia, a surface cooling anomaly is found in the high AOD region. The magnitude of the cooling is smaller compared to that in the Indian subcontinent. As shown in Kim *et al* (2007), the radiative forcing of sulfate, which is a major constituent of aerosols over East Asia (see table 1), reduces rainfall through dynamical feedback. As a result, surface cooling by aerosols is partially compensated by reduced cloudiness in East Asia. Remarkably, a pronounced surface warming anomaly is found over the TP, especially the western Himalayas, where the climatological snow cover is more extensive compared to elsewhere in the TP. The land surface warming extends over large regions, covering northwestern Asia, including Kazakhstan and Pakistan, and northeastern China, including Mongolia. As shown in the following, the pronounced surface warming (>1°C) over the WTP and the Himalayas is directly linked to the accelerated snow melt over that region. Results from experiments with the same model but with non-absorbing aerosols, i.e. sulfate, show that there is no surface warming, but actually increased snow cover over the TP (see supplementary material, Fig. S1 available at stacks.iop.org/ERL/5/025204/mmedia).

Associated with the aerosol-induced pre-monsoon surface warming over TP are significant changes in the large-scale environment. These include widespread warming in the near-surface air over the TP and adjacent region, most pronounced (>0.9°C) over the WTP, coupled to the cooling over central and eastern India (figure 3(a)); and enhanced precipitation (figure 3(b)), more mid-to-upper tropospheric moisture (figure 3(c)), and increased cloudiness (figure 3(d)) over northern Indian and the foothills of the Himalayas. Since the warming regions are not anywhere near the centers of high AOD, and have much larger spatial scale than the aerosol direct forcing (figure 1(a)), the warming cannot be attributed to direct aerosol radiative forcing alone, but rather arises from atmospheric feedback processes, and, as illustrated below, is associated with the EHP mechanism. The EHP has been described in previous studies and is briefly described below in the context of TP warming and snow melt.

During boreal spring, dusts are transported from the deserts west of the Indian subcontinent, and accumulate over the IGP, against the foothills of the Himalayas. As dust storms pass through the IGP, the dust aerosols sweep up BC from local emissions in the IGP, resulting in highly absorbing dust particles (Eck *et al* 2005). Both the dust and BC are forced up the Himalayan slopes, by the large-scale monsoon low-level flow, and by dry pre-monsoon convection, accumulated along the foothills of the Himalayas, with the finer particles reaching the top of the TP and above. The elevated dust and black carbon absorbs solar radiation and heats the atmosphere around the slopes of the TP (figure 4(a)), further enhancing the motion up and along the TP slopes. As the late spring and early summer (April through mid-June) approaches, the increased low-level southwesterly brings in additional moisture from the Arabian Sea and the Indian Ocean to northern India and the Himalayan foothills (figure 4(b)). The enhanced moisture increases convective instability and spurs deep convection and cloudiness over northern India. The condensation heating from deep convection amplifies the seasonal warming over the TP, resulting in a widespread upper tropospheric warming anomaly over the TP. The increase in cloudiness associated with the enhanced convection is, in large part, responsible for the large surface cooling found over central and northern India (figure 2). The aforementioned features comprise the essence of the EHP effect (Lau *et al* 2006).

3.2. EHP-induced snow melt, and changes in surface energy balance

Because of its coarse resolution, the model shows a rather simple high mountain snow distribution, with only substantial snow cover in the western Himalayas, with a maximum thickness of over 80 cm of snow in April–May (figure omitted). The much smaller scale snowpack, and glacier

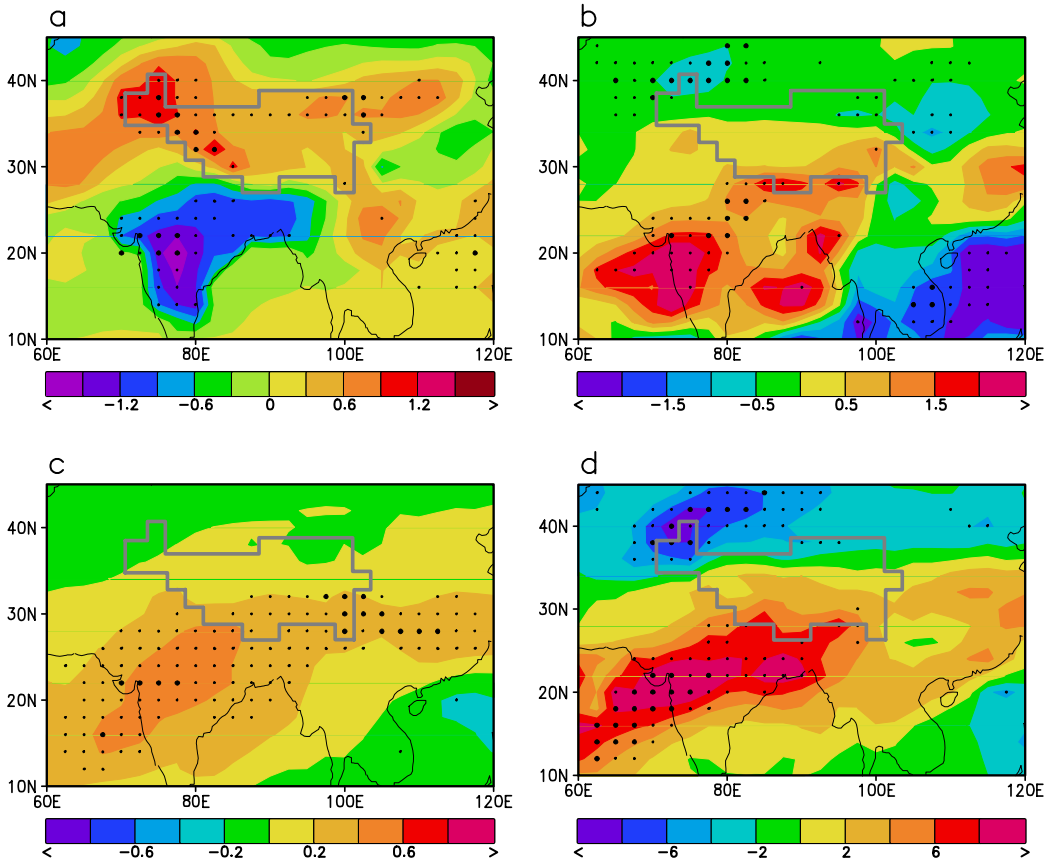

Figure 3. Spatial patterns of (a) 2 m air temperature (°C), (b) precipitation (mm/day), (c) layer mean specific humidity between 700 and 300 hPa (g kg^{-1}), and (d) total cloud cover (%) differences defined as the monthly mean difference between AA and NA runs for May. The gray line outlines the boundary of TP. Grid points with statistical confidence levels exceeding 5 and 1% are indicated by small and large closed circles, respectively. The model outline of the TP is shown by the solid gray line.

lakes observed in the ETP, are not resolved. The region of most pronounced anomalous snow melt coincides with the maximum surface warming anomaly (see figure S1 available at stacks.iop.org/ERL/5/025204/mmedia). From table 2, significant EHP-induced accelerated snow melt occurs in May over the TP, with almost all contribution from the western Tibetan Plateau (WTP), and a relatively very small amount from the eastern Tibetan Plateau (ETP). Here, WTP and ETP are defined respectively as the domain west and east of the 90° E longitude, within the outline of the TP, bounded by the thick gray lines in figures 1–3. To estimate the rate of reduction of snow amount, we have computed the change in 'effective surface albedo' in terms of the ratio of reflected to incoming solar radiation at the surface. The decrease in effective surface albedo is due to both reduction in snow depth and snow aging, as well as the exposure of the underlying darker soil when snow is melted. Since almost all the snow cover anomaly occurs in the WTP (table 2), only the WTP snow cover changes will be discussed. Figure 5 shows the time series of (a) the climatology and (b) the reduction in effective surface albedo for the WTP, and for the domains where the mean snow depth is greater than or equal to 10 and 30 cm. The sizes of these domains are determined from the April climatology and remain fixed in computations of the effective surface albedo. Figure 5(a) shows that, climatologically, the surface albedo over the entire TP reduces from about 0.5 to 0.2 between April and June. The relatively low effective albedo is due to the fact that a large part of the TP remains snow free during this period. Over the domains with deeper snow, the climatological surface albedo reduces from 0.7 to 0.2 from April to June. Irrespective of the climatological mean snow depth chosen to define the snow field, the time variations of the anomalous surface albedo (figure 5(b)) are similar. The deeper snow fields, which cover smaller areas, have the larger percentage reduction. The maximum reduction for the 30 cm snowline is approximately 8–10%.

Table 2. Area mean snow depth anomalies, defined as monthly mean difference between AA and NA runs, over the TP, the WTP, and the ETP. Climatological mean values of snow depth from the control experiment are shown in parentheses. The WTP and ETP are defined with respect to the 90° E longitude line. Units are in centimeters. Boldface type indicates values statistically significant at least at the 5% level. (∗) indicates values significant at the 1% level.

	TP	WTP	ETP
April	**−0.81** (33.82)	**−1.27** (62.12)	−0.05 (0.81)
May	**−2.24*** (13.22)	**−3.63*** (24.47)	−0.01 (0.09)
June	**−0.73*** (2.03)	**−1.18*** (3.76)	−0.00 (0.01)

To facilitate the discussion, we divide the aerosol-induced snow melting processes into three phases. The anomalous melting of snow cover starts slowly in early April, and grows

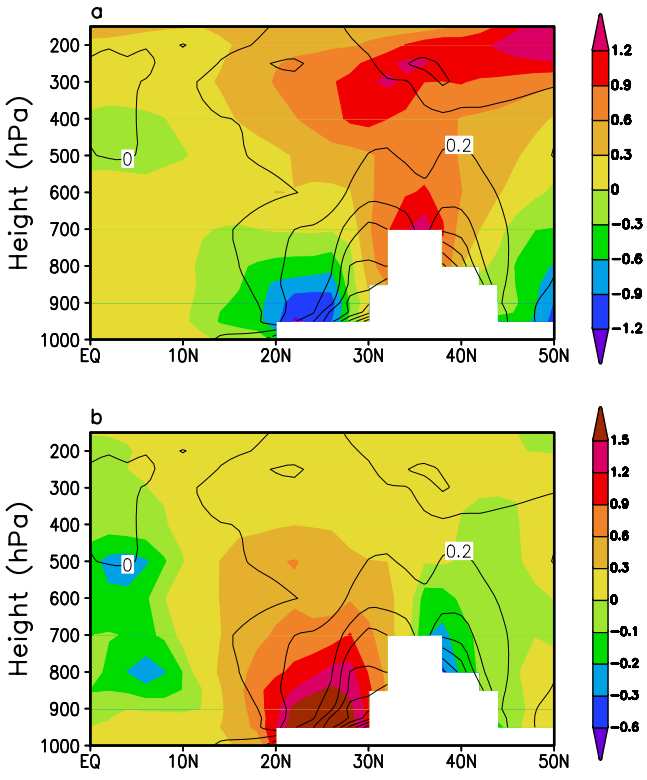

Figure 4. Latitude–height cross-section of the simulated difference (AA–NA) of the short-wave radiative forcing (contour, °C/day) and (a) temperature (°C) and (b) specific humidity (g kg^{-1}) averaged between 70 and 100° E for May. The model profile of the TP is indicated by the white shading.

steadily through the beginning of May (phase I). From around 3 May, the snow melt accelerates, reaching a maximum in mid-May (phase IIA). The snow melt slows down, and the snow cover reaches a minimum, from 18 May to 11 June (phase IIB). Subsequently, from 11 June to 26 (phase III), the aerosol effect diminishes, and snow cover recovers in response to enhanced cold precipitation over the TP (see discussion below).

The timing of the WTP snow melt is closely linked to responses in temperature and the water cycle over the TP to the EHP effect. During phase I, the atmosphere and the land surface temperature increase moderately, with the atmosphere warming generally greater than and leading that at the surface (figures 6(a) and (b)). The warming has a strong east–west contrast, more pronounced in the WTP than in the ETP. At this time, the air over the TP is relatively dry (figure 6(c)). Rainfall and cloudiness are reduced over the TP (figures 6(d) and (e)), because of increased atmospheric stability, with the atmosphere warming faster than the land, i.e. the semi-direct effect (Hansen *et al* 1997). The rapid snow melt during phase IIA occurs as the monsoon season approaches, and more moisture is available to fuel the EHP effect, as can be seen by the rapid rise in atmospheric and land surface temperature and available moisture (figures 6(a)–(c)). Precipitation and cloudiness are enhanced first over the ETP downstream of the southwest monsoon flow due to the EHP effect. During phase IIB, atmospheric moisture, precipitation and cloudiness increases substantially over both the WTP and ETP, and the atmosphere and surface temperature anomalies are decreased, and snow melting is slowed down by increasing surface evaporation. The increase in precipitation in the WTP continues into phase III. Because of the high altitude of the TP, the precipitation is likely to be in the form of snow, and is partly responsible for the recovery (phase III) of the snow cover in the WTP.

The causes of the anomalous surface warming and snow melt in the TP can be better understood in terms of the induced changes in the surface energy balance. The anomalous surface short-wave (SW) and long-wave (LW) fluxes (figure 7(a) and (b)) are closely linked to the variations in cloudiness (figure 6(e)). During periods of reduced

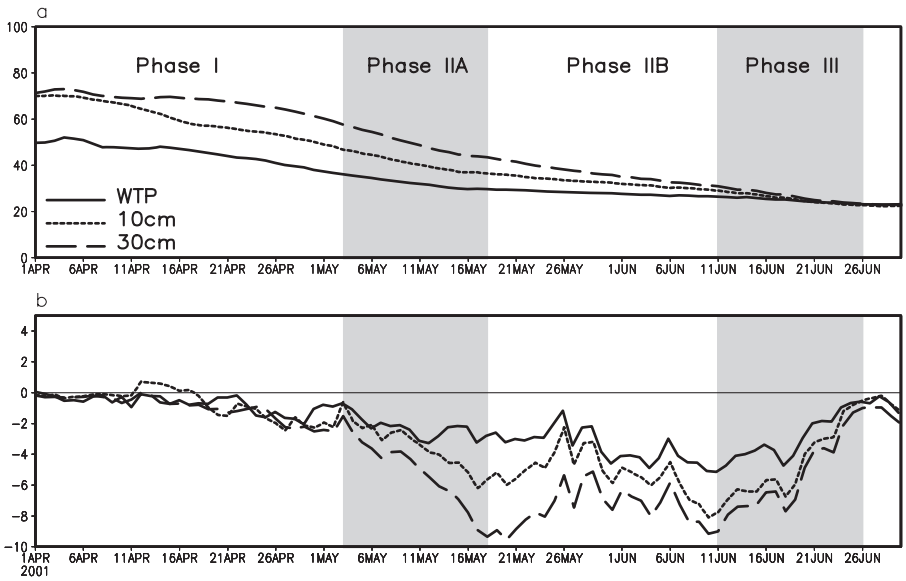

Figure 5. Time variation of (a) area mean climatological surface albedo (%) in NA run, and (b) relative percentage change of surface albedo (%) in AA run as compared to NA run over the WTP (solid line). Dotted and dashed lines are albedo changes from the region where the climatological snow depths are larger than or equal to 10 cm (dotted line) or 30 cm (dashed line), respectively.

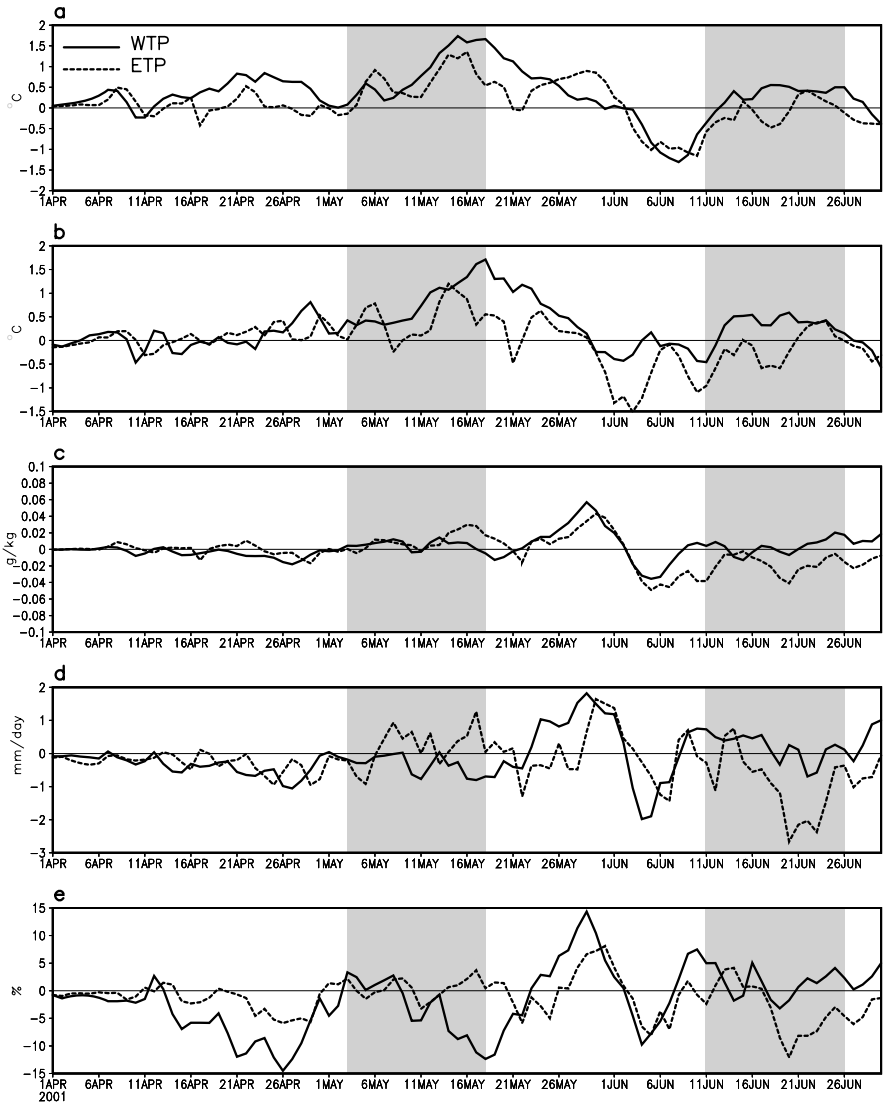

Figure 6. Time series of AA-minus-NA daily mean of (a) surface air temperature (°C), (b) surface skin temperature (°C), (c) specific humidity (g kg^{-1}) in upper troposphere between 700 and 300 hPa, (d) precipitation (mm/day), and (e) total cloud fraction (%) over the WTP (solid line) and the ETP (dotted line).

(enhanced) cloudiness, warming (cooling) of the surface by downward SW is enhanced, and LW cooling (warming) is increased. During phase I, except briefly in 1–6 April, the SW warming from reduced cloudiness is largely over-compensated by LW cooling, with a net radiative cooling effect of less than 5 W m^{-2}. During this phase, the anomalous surface warming and snow melt are initiated by a transfer of sensible heat (SH) from atmosphere to land, i.e. negative SH flux (figure 7(e)), because of the more rapid warming of the atmosphere compared to the surface. As the snow thins and the snow cover area shrinks, surface evaporation is reduced, due to the exposure of the dry soil, as indicated by the negative latent heat (LH) flux (figure 7(d)), resulting in more heating of the surface. A positive feedback ensues, with more surface heating leading to faster snow melt, and further reduction in surface evaporation. This is evident in the large negative surface evaporation anomaly (figure 7(d)) at the end of phase I, immediately preceding phase IIA. In addition, the increased moisture transport from the foothills to the TP due to EHP also contributes to the negative LH flux in phase IIA, which witnesses a net negative LH flux of 5–10 W m^{-2} over both the WTP and ETP (figure 7(d)). The large increase in LH flux (negative LH) from atmosphere to land outweighs the net radiative cooling, as evident in the pronounced net energy gain by the surface (figure 7(f)) in phase IIA, and is largely responsible for the faster snow melt. During phase IIB, accompanying the onset of precipitation over the WTP, moisture in the exposed bare soil is increased, and the land cools by increased evaporation (figure 7(d)), causing a slow-down in the warming of the surface (figure 6(b)) and in the melting of the snow (figure 5). During phase III, SH from atmosphere to land (negative upward SH fluxes in figure 7(e)) continues to maintain the surface warming process, which is damped by evaporative cooling (positive LH flux in figure 7(d)), and net radiative cooling (reduced downward net radiative flux in figure 7(c)).

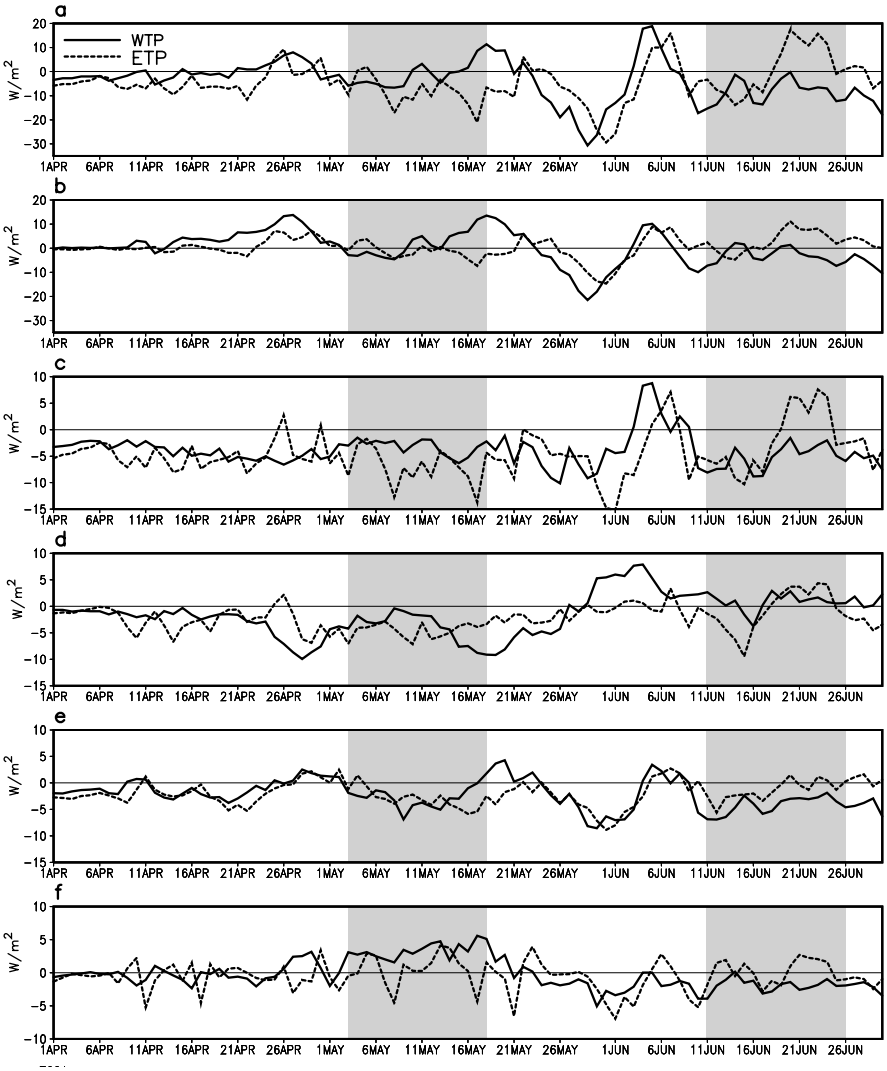

Figure 7. Time series of AA minus NA daily mean of (a) net short-wave, (b) net long-wave, (c) net radiative fluxes, (d) latent heat flux, (e) sensible hear flux, and (f) net surface flux at the surface over the WTP (solid line) and the ETP (dotted line). Units are W m^{-2}. Positive flux indicates downward for short-wave (a), net radiative (c), and net heat fluxes (f), while positive flux indicates upward for long-wave (b), latent (d) and sensible (e) fluxes.

4. Conclusion

From numerical experiments with the NASA fvGCM, we found that the heating of the troposphere by elevated dust and black carbon aerosols in the boreal spring can lead to widespread enhanced land–atmosphere warming, and accelerated snow melt in the Himalayas and Tibetan region. The warming and snow melt are most pronounced in the WTP region in late April to mid-May, where the climatological snow cover is deeper and more extensive compared to the ETP. The surface short-wave and long-wave radiative fluxes are closely linked to the variations of cloudiness, and largely offset each other, with an overall net cooling effect. The surface heating and accelerated snow melt stem from an effective transfer of heat from atmosphere to land through sensible and latent heat fluxes (∼5–10 W m^{-2}), outweighing the net radiative (SW + LW) cooling effect (<5 W m^{-2}).

Climatologically, during boreal spring, the surface of the TP is heated by increased seasonal solar radiation, and the atmosphere over the TP by sensible heat flux, and to a lesser degree by latent heat flux (Yanai and Wu 2006, Yanai *et al* 1992). Our results suggest that, as a response to radiative forcing by dust and black carbon in the Indo-Gangetic Plain and Himalaya foothills, the atmosphere over the TP is anomalously heated, and moistened via the EHP effect (Lau *et al* 2006). The warm and moist atmosphere overlying the TP land surface causes a reduction in surface sensible and latent heat fluxes from land to atmosphere, i.e. a net heat gain by the land surface. The net heat gained is used for melting more snow over the TP and the Himalayas. Effectively, the anomalous atmosphere heat energy induced by solar heating of aerosols is transfer from atmosphere to land to enhance the seasonal warming of the land surface and the melting of snow in the region.

In the real world, the snow-darkening effect by deposition of soot and dust on mountain glaciers is likely to add to the EHP effect in leading to even more accelerated snow melt. In addition, the EHP could be an important mechanism

for transport of pollutants from the IGP to high altitudes by enhanced convection, and affect both dry and wet deposition of dust and black carbon on Tibetan glaciers. Preliminary results from recent work with the fvGCM show that the EHP effect is likely to be amplified by including the aerosol microphysical effects on clouds and precipitation (Sud *et al* 2009). For future work, the EHP, snow-darkening effects, and the impact of microphysical effects of aerosols need to included in a high-resolution climate model capable of resolving the complex terrains and orographic convection over the Himalayas and TP regions.

Acknowledgments

This work is supported by the Interdisciplinary Program, NASA Headquarters, program manager Dr H Maring. This work is partially supported by a grant (CATER 2009-1147) from the Korea Meteorological Administration Research and Development Program of the Republic of Korea.

References

Atlas R, Reale O, Shen B W, Lin S J, Chern J D, Putman W, Lee T, Yeh K S, Bosilovich M and Radakovich J 2005 Hurricane forecasting with the high-resolution NASA finite volume general circulation model *Geophys. Res. Lett.* **32** L03807

Chin M, Chu A, Levy R, Remer L, Kaufman Y, Holben B N, Eck T, Ginoux P and Gao Q 2004 Aerosol distribution in the Northern Hemisphere during ACE-Asia: results from global model, satellite observations, and Sun photometer measurements *J. Geophys. Res.* **109** D23S90

Chin M, Ginoux P, Kinne S, Torres O, Holben B N, Duncan B N, Martin R V, Logan J A, Higurashi A and Nakajima T 2002 Tropospheric aerosol optical thickness from the GOCART model and comparisons with satellite and Sun photometer measurements *J. Atmos. Sci.* **59** 461–83

Chou M D and Suarez M J 1994 An efficient thermal infrared radiation parameterization for use in general circulation models. *NASA Tech. Memo. 104606* 3 p 85 [NTIS N95-15745]

Chou M D and Suarez M J 1999 A solar radiation parameterization for atmospheric studies *NASA Tech. Memo. 104606* 15 p 38

Dai Y *et al* 2002 The common land model (CLM) *Bull Am. Meteor. Soc.* **84** 1013–23

Duan A M, Wu G X, Zhang Q and Liu Y M 2006 New proofs of the recent climate warming over the Tibetan Plateau as a resultt of increased greenhouss gases emissions *Chin. Sci. Bull.* **51** 1396–400

Eck T F *et al* 2005 Columnar aerosol optical properties at AERONET sites in central eastern Asia and aerosol transport to the tropical mid-Pacific *J. Geophys. Res.* **110** D06202

Flanner M G, Zender C S, Hess P G, Mahowald N M, Painter T H, Ramanathan V and Rasch P J 2009 Springtime warming and reduced snow cover from carbonaceous particles *Atmos. Chem. Phys.* **9** 2481–97

Flanner M G, Zender C S, Randerson T J and Rasch P J 2007 Present-day climate forcing and response from black carbon in snow *J. Geophys. Res.* **112** D11202

Gautam R, Hsu N C, Lau K M, Tsay S C and Kafatos M 2009 Enhanced pre-monsoon warming over the Himalayan-Gangetic region from 1979–2007 *Geophys. Res. Lett.* **36** L07704

Ginoux P, Chin M, Tegan I, Prospero J, Holben B N, Dubovik O and Lin S J 2001 Sources and distributions of dust aerosols simulated with the GOCART model *J. Geophys. Res.* **106** 20225–73

Hansen J, Sato M and Ruedy R 1997 Radiative forcing and climate response *J. Geophys. Res.* **102** 6831–64

He Y, Zhang Z, Theakstone W H, Chen T, Yao T and Pang H 2003 Changing features of the climate and glaciers in China's monsoonal temperate glacier region *J. Geophys. Res.* **108** 4530

IPCC 2007 *Climate Change 2007: The Physical Science Basis. Contribution of Working Group I to the Fourth Assessment Report of the Intergovernmental Panel on Climate Change* ed S Solomon, D Qin, M Manning, Z Chen, M Marquis, K B Averyt, M Tignor and H L Miller (Cambridge: Cambridge University Press)

Jain S K 2008 Impact of retreat of Gangotri glacier on the flow of Ganga River *Curr. Sci.* **95** 1012–4

Kang S C, Wake C P, Qin D H, Mayewski P A and Yao T D 2000 Monsoon and dust signals recorded in Dasuopu glacier, Tibetan Plateau *J. Glaciol.* **46** 222–6

Kehrwald N M, Thompson L G, Tandong Y, Mosley-Thompson E, Schotterer U, Alfimov V, Beer J, Eikenberg J and Davis M E 2008 Mass loss on Himalayan glacier endangers water resources *Geophys, Res. Lett.* **35** L22503

Kim M K, Lau K M, Kim K M and Lee W S 2007 A GCM study of effects of radiative forcing of sulfate aerosol on large scale circulation and rainfall in East Asia during boreal spring *Geophys. Res. Lett.* **34** L24701

Kulkarni A V, Bahuguna I M, Rathore B P, Singh S K, Randhawa S S, Sood R K and Dhar S 2007 Glacial retreat in Himalaya using Indian remote sensing satellite data *Curr. Sci.* **92** 69–74

Kulkarni A V, Mathur P, Rathore B P, Alex S, Thakur N and Kumar M 2002 Effect of global warming on sow ablation pattern the Himalayas *Curr. Sci.* **83** 120–3

Lau K M *et al* 2008 The joint aerosol-monsoon experiment: a new challenge in monsoon climate research *Bull. Am. Meteor. Soc* **89** 369–83

Lau K M and Kim K M 2006 Observational relationships between aerosol and Asian monsoon rainfall, and circulation *Geophys. Res. Lett* **33** L21810

Lau K M, Kim M K and Kim K M 2006 Asian monsoon anomalies induced by aerosol direct forcing: the role of the Tibetan Plateau *Clim. Dyn.* **26** 855–64

Lin S J 2004 A vertically Lagrangian finite-volume dynamical core for global models *Mon. Weather Rev.* **132** 2293–307

Liu X D and Chen B 2000 Climate warming in the Tibetan Plateau during recent decades *Int. J. Climatol.* **20** 1729–42

Manabe S and Broccoli A J 1990 Mountains and arid climate of mid-latitudes *Science* **247** 192–5

Oerlemans J 2005 Extracting climate signals from 169 glacier records *Science* **308** 675–7

Prasad A K and Singh R P 2007 Changes in Himalayan snow and glacier cover between 1972 and 2000 *EOS Trans. Ann. Geophys. Union* **88** 326

Prasad A K, Yang K H S, El-Askary H M and Kafatos M 2009 Melting of major glaciers in the western Himalayas: evidence of climatic changes from long term MSU derived tropospheric temperature trend (1979–2008) *Ann. Geophys.* **27** 4505–19

Raina V K and Sangewar C 2007 Siachen glacier of Karakorum Mountains, Ladakh, its secular retreat *J. Geol. Soc. India* **70** 11–6

Ramana M V, Ramanathan V, Podgorny I A, Pradhan B and Shrestha B 2004 The direct observations of large aerosol radiative forcing in the Himalayan region *Geophys. Res. Lett.* **31** L05111

Ramanathan V, Ramana M V, Roberts G, Kim D, Corrigan C E, Chung C E and Winker D 2007 Warming trends in Asia amplified by brow cloud solar absorption *Nature* **448** 575–8

Ren J W, Jing Z F, Pu J C and Qin X 2006 Glacier variations and climate change in central Himalaya over the past few decades *Ann. Glaciol.* **43** 218–22

Shrestha A B, Wake C P, Mayewski P A and Dibb J E 1999 Maximum temperature trends in the Himalaya and its vicinity:

an analyais based on temperature records from Nepas for the period 1971–94 *J. Clim.* **12** 2775–86
Sud Y C and Walker G K 1999 Microphysics of clouds with relaxed Arakawa-Schubert scheme (McRAS). Part II: implementation and performance in GEOS II GCM *J. Atmos. Sci.* **56** 3221–40
Sud Y C and Walker G K 2003 Influence of ice-phase physics of hydrometeors on moist convection *Geophys. Res. Lett.* **30** 1758
Sud Y C, Wilcox E, Lau K M, Walker G K, Liu X H, Nenes A, Lee D, Kim K M, Zhou Y and Bhattacharjee PS 2009 Sensitivity of boreal summer circulation and precipitation to atmospheric aerosols in selected regions. Part I: Africa and India *Ann. Geophys.* **27** 3989–4007
Waliser D E, Lau K M and Kim J H 1999 The influence of coupled sea surface temperatures on the Madden-Julian oscillation: a model perturbation experiment *J. Atmos. Sci.* **56** 333–58
Yanai M, Li C and Song Z 1992 Seasonal heating of the Tibetan Plateau and its effects on the evolution of the Asian summer monsoon *J. Meteor. Soc. Japan* **70** 319–51
Yanai M and Wu G W 2006 *Effects of the Tibetan Plateau in the Asian Monsoon* ed B Wang (New York: Springer) pp 513–49
Yasunari T J, Bonasoni P, Laj P, Fujita K, Vuillermoz E, Marinoni A, Cristofanelli P, Duchi R, Tartari G and Lau K M 2009 Preliminary estimation of black carbon deposition and its possible impact on snow albedo changes over Himalayan glaciers during pre-monsoon season *Geophys. Res. Lett.* submitted
Yu H, Chin M, Winker D M, Omar A H, Zhaoyan L, Kittaka C and Diehl T 2010 Global view of aerosol vertical distributions from CALIPSO lidar measurement and GOCART simulations: regional and seasonal variations *J. Geophys. Res.* submitted